Applied Physics A (2021) 127:432
https://doi.org/10.1007/s00339-021-04533-6

Applied Physics A
Materials Science & Processing

A differential model for the hysteresis in magnetic shape memory alloys and its application of feedback linearization

Haoyuan Du[1] · Yuxiang Han[1] · Linxiang Wang[1] · Roderick Melnik[2]

Received: 17 February 2021 / Accepted: 15 April 2021 / Published online: 19 May 2021

Abstract
Magnetic shape memory alloys (MSMAs) are materials with strong nonlinearity, which will show hysteresis when it works. In the current paper, a differential model is proposed to describe the hysteresis in MSMAs caused by magnetic field induced martensite reorientation based on Landau theory of phase transitions. First, the three-dimensional model is simplified into a one-dimensional case, and the hysteresis in MSMAs is described by three martensite variant orientations. Then, a traditional Landau free energy is introduced, and the traditional Landau model is obtained by using the Euler–Lagrange equation. However, it is found that the prediction accuracy of the model is not ideal compared with the experimental data. Thus, an improved model is proposed, and the traditional Landau free energy is replaced by a function that can be determined by the easily measured physical quantities in the experimental curve. Numerical experiments show that the prediction effect of the improved model is much better than the traditional Landau model, and the stress dependence is also demonstrated. Moreover, the proposed improved model has the advantages for dynamic analysis and control with its differential form. Therefore, the frequency dependence of the improved model is demonstrated and a feedback linearization control methodology is proposed to make the system develops in the desired trajectory.

Keywords Magnetic shape memory alloy · Hysteresis dynamics · Differential equations · Martensite reorientation · Feedback linearization

1 Introduction

As a new type of promising smart material, magnetic shape memory alloys (MSMAs), generally named ferromagnetic shape memory alloys (FSMAs), were found in 1996 [1–4]. Compared with the traditional smart materials, such as piezoelectric materials and shape memory alloys (SMAs), MSMAs have better performance. For example, the magnetic field induced strain (MFIS) in MSMAs can be reached as much as 10%, and it is reversible [5, 6]. In typical MSMA materials, such as NiMnGa, there are mainly two phases: cubic austenite and tetragonal twin martensite variants, as shown in Fig. 1 [7]. There are three possible martensite variants, and each has two possible magnetization orientations as the arrows indicate. In martensite variants, $\boldsymbol{a}$ refers to the long edges, and $\boldsymbol{c}$ refers to the short one. Note that the $\boldsymbol{c}$ axis is the magnetic easy axis which means that the martensitic variants are preferred to be magnetized [7]. Similar to other smart materials, MSMAs also have strong nonlinearity which is mainly caused by martensite reorientation. The reorientation of the martensite variants can be induced by the magnetic and mechanical fields [7–13].

There are mainly three applications of MSMAs. The first case is the temperature-induced phase transition of MSMAs [10, 11]. At high temperature (above Curie temperature), the MSMA is in a cubic austenite phase. When the temperature is cooled to a lower temperature, phase transition will be induced, and the austenite phase will transfer to the twin martensite phase. In this process, the strain will change, thus there can be displacement output [5]. However, as the temperature is hard to control, the application of temperature-induced MSMA phase transition is rare, which is similar to SMA.

✉ Linxiang Wang
wanglx236@zju.edu.cn

[1] State Key Laboratory of Fluid Power and Mechatronic Systems, Zhejiang University, Hangzhou 310027, People's Republic of China

[2] MS2Dicovery Interdisciplinary Research Institute, Wilfrid Laurier University, Waterloo, ON N2L 3L5, Canada

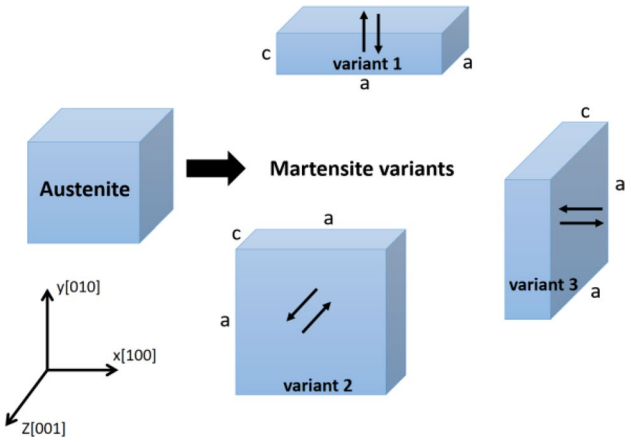

Fig. 1 Crystal structure of austenite and martensite variants in MSMA

The second case is the magnetic field induced martensite reorientation in MSMAs. Below the Curie temperature, only twin martensites exist in MSMAs as shown in Fig. 1. With the application of magnetic field, the magnetic easy axis (*c* axis) will turn to the magnetic field direction. In this process, the magnetic field induced strain (MFIS) can reach as much as 10% [5, 6, 10]. The direction of elongation is perpendicular to the magnetic field because *c* axis is the short edge. MSMA actuator is based on this principle and can achieve large output. At the same time, due to the small size of MSMAs (mm level), this kind of actuator has a wide application prospect in many fields such as micro-robot.

The last case is to use stress or strain induced martensite reorientation in MSMAs [6, 8, 13–15], which is very similar to ferroelectric materials [16, 17]. The induced martensite reorientation will cause the change of the magnetization along the long axis (***a*** axis). A pickup coil is around the MSMA specimen. According to Faraday's law of induction, there will be induced voltage in the coil [7]. Then the generated electric energy can be dissipated or harvested by an external circuit, which is similar to the piezoelectric shunt damping technique [18]. According to this principle, MSMA can be used for energy dissipation or energy harvesting. Therefore, MSMAs can be used for acoustic wave absorption, vibration attenuation and power supply of low-powered electrical appliances with a very broad application prospect.

From the above, it can be seen that MSMA is one of the most promising smart materials. Thus, it is necessary to establish its constitutive model and make it convenient to control in engineering applications. Many constitutive models of MSMAs have been proposed so far [7, 11–14, 19–22]. A thermodynamically phenomenological constitutive model was proposed by B. Kiefer in 2005 [11]. By using the state variables, the magnetic shape memory effect (MSME) caused by martensite reorientation could be modeled. Magnetocrystalline anisotropy energy and Zeeman energy are introduced to describe the magnetism contribution to free energy. Besides, the MSMA was modeled to describe its magneto-mechanical property by using the variational approach [19]. The constitutive form for the effective magnetization vector was proposed based on experimental results. Considering the energy dissipations during the martensite reorientation process, the total energy functional in the magneto-mechanical system was constructed. This model was confirmed to capture the features of experimental curves successfully. Moreover, a framework was presented to describe the frequency-dependent energy harvesting with MSMAs by Sayyaadi [20]. The reorientation-induced strain was defined by the hyperbolic hardening function, and the dynamic effects were considered by using the diffusion equation. Finally, it was found that energy harvesting was mainly determined by dynamic effects, particularly in high frequency. Rui et al. [21] used the Krasnosel'skii-Pokrovskii (KP) model, in which the Elman neural network was used to determine the density function, to describe the hysteresis characteristics of MSMA actuator. The results show that the error of KP model identified by Elman neural network is much smaller than that of using the recursive least square method, which demonstrates the effectiveness of the proposed model. Zhou [22] investigated the characteristics of hysteresis behavior under different input signals in MSMA. A rate-dependent hysteresis model was constructed by using NARMAX model based on the diagonal recurrent neural network (DRNN), and the play operator was adopted as the exogenous variable function of the NARMAX model. Finally, excellent modeling performance was shown by comparing with experimental results.

Several models above are representative and meaningful, but there are still some drawbacks, such as expensive computation and low efficiency. For example, the model in Ref. [11] is in a partial differential equation (PDE) form, which is relatively complex and needs more computational cost than the ordinary differential equation (ODE) model. And it is still a great challenge to build a model that takes both accuracy and efficiency into account. Due to the similar mechanism of hysteresis, Landau theory of phase transition has been widely used in ferroelectric and ferromagnetic materials [23–30]. A differential model for modeling the hysteresis in ferromagnetic materials has been proposed by our research team [24]. This model can describe the magnetization orientation switching well by using a phenomenological theory, which is based on the Landau theory of phase transition. The hysteretic dynamics of the switching process are accurately captured. However, in the application of ferromagnetic materials, especially in MSMAs, the coupling of magnetic and stress fields usually needs to be considered, which is not mentioned in the previous model. Therefore, in the current paper, based on the single crystal model in

Ref. [24], we introduce the stress term and establish a model which can be used to describe the stress related characteristics of MSMA. An ordinary differential equation (ODE) model of MSMAs is proposed based on the Landau theory of phase transitions, and the hysteretic dynamics in MSMAs are associated with the martensite reorientation dynamics. Then, we improved the traditional Landau model and proposed an improved model, which has higher accuracy. At the same time, the stress and frequency dependence of the model are demonstrated, which are very important in the application of MSMAs. For the ordinary differential equation (ODE) form, our model has the advantages of simple form, high efficiency and low computational cost. Moreover, a feedback linearization methodology is proposed to eliminate the hysteresis in the model. The paper is organized as follows. In Sect. 2, a traditional Landau model is proposed. Then this model is revised to form an improved model in Sect. 3 to improve the accuracy, and the stress dependence is demonstrated. Moreover, the frequency dependence of the improved model is demonstrated in Sect. 4. Finally, due to the differential form of the model, a feedback linearization methodology is proposed to ensure the system outputs follow the desired trajectory in Sect. 5.

2 Traditional Landau model and validation

2.1 Reduced structure and Landau theory

In most cases, the shape of MSMAs is a rod, and the direction of applied magnetic field is perpendicular to the expected strain output direction [2, 6, 11, 12]. Only the most commonly observed martensite variants are considered. Therefore, considering the efficiency and its application in engineering, the three-dimensional crystal structure of martensite variants is reduced as a one-dimensional analog as shown in Fig. 2, in which Fig. 7.2 in Ref. [2] is used as a reference. As shown in Fig. 2, there are three martensite variants exist: V_2^-, V_1 and V_2^+. A typical magnetic field induced variants reorientation of MSMAs can be described as shown in Fig. 2. Initially, suitable biased compress stress (σ_{xx}) is applied along the length of the MSMA specimen to make it

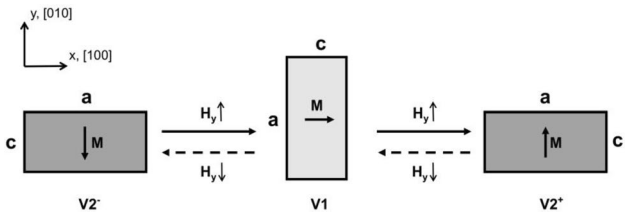

Fig. 2 Schematic of the magnetic field induced variants reorientations in one-dimensional

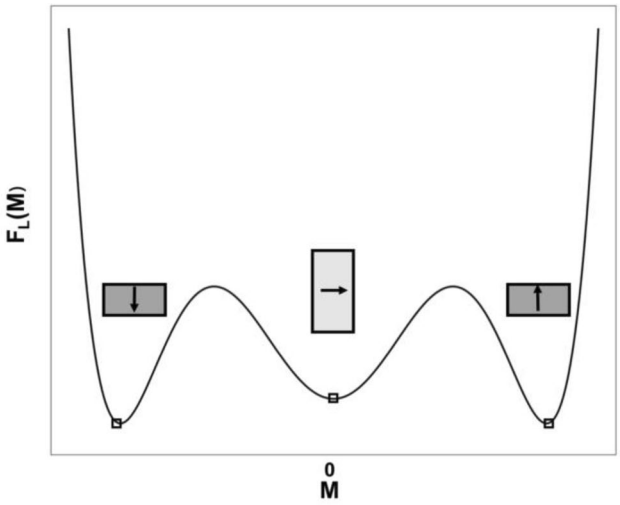

Fig. 3 Constructed Landau free energy function

in a single variant configuration (V_1) [2]. Then decrease the stress to the desired level to preserve that configuration and keep it constant for the following experiment. Next, with a sufficiently large magnetic field H_y in the [010]-direction ($H_y\uparrow$) applied to the MSMA specimen, V_1 flips to the V_2^+ since the magnetic easy axis (c axis) is favored in this direction of the H_y, and there will be a large strain output in the x-axis direction [31]. When the direction of H_y is reversed ($H_y\downarrow$), V_2^+ will flip back to V_1. When H_y increases further in this direction ($H_y\downarrow$), V_1 will flip to V_2^-. Reducing the H_y, V_2^- returns to the initial V_1 with the application of σ_{xx}. The above is a simplified case of typical martensite reorientation. It can be seen that the simplified quasi one-dimensional model can well describe this process by using these three martensite variants. For more details of the process of the martensite reorientation, interested readers can refer to Ref. [2, 10, 11, 14].

Then according to the Landau theory of phase transitions [23, 31], the various magnetization orientations and martensite reorientations can be characterized by the Landau free energy function. This function needs to be non-convex and has multiple local minima. And each minimum corresponds to one magnetization orientation. In this section, M is chosen as the order parameter, and the Landau free energy function is constructed as shown below:

$$\phi_M = \frac{A_2}{2}M^2 + \frac{A_4}{4}M^4 + \frac{A_6}{6}M^6, \tag{1}$$

where M is the magnetization, and A_2, A_4, A_6 are the corresponding Landau coefficients which are related to the material properties.

By choosing proper Landau coefficients, the Landau free energy function can be easily constructed, as shown

in Fig. 3. It can be seen that the prior requirements are satisfied by this function. This curve forms three wells around the minima that correspond to the three proposed martensite variants in Fig. 2. If the MSMA firstly in V_2^- state, it will need enough energy to overcome the energy barrier to reorient to V_1 and further to V_2^+.

2.2 Macroscopic differential model

For the reduced one-dimensional analog, the Helmholtz free energy $\psi(M,\varepsilon)$ can be constructed as following for the MSMAs:

$$\psi(M,\varepsilon)=\frac{A_2}{2}M^2+\frac{A_4}{4}M^4+\frac{A_6}{6}M^6+\frac{k}{2}\varepsilon^2+\frac{\beta}{2}\varepsilon M^2, \tag{2}$$

where k and β are material constants, respectively.

In the current paper, the dynamics of the system states are considered to approach their equilibrium and therefore, the dynamics of the martensite reorientations in MSMAs can be modeled. The response of the system in the magnetic and mechanical fields is described by magnetization (M) and strain (ε), respectively. In this modeling, the microstructure caused by the martensite reorientations in the specimen is not considered and ignored, and both M and ε are assumed to be lumped (uniform in the specimen). The system states can be uniquely determined by specifically given values (M and ε). Therefore, the dynamic system is low-dimension, and Lagrange's equations can be used to describe the motion equations.

Out of this purpose, the potential energy function $V(M,\varepsilon)$ can be constructed combined with the Helmholtz free energy in Eq. (2)** as:

$$V(M,\varepsilon)=\psi(M,\varepsilon)-HM-\varepsilon\sigma, \tag{3}$$

where H and σ are magnetic field intensity and stress, HM and $\varepsilon\sigma$ are the applied magnetic energy and mechanical energy, respectively.

The kinetic energy can be taken as:

$$U=\frac{1}{2}\left(I_M\left(\frac{\mathrm{d}M}{\mathrm{d}t}\right)^2+I_\varepsilon\left(\frac{\mathrm{d}\varepsilon}{\mathrm{d}t}\right)^2\right), \tag{4}$$

where I_M and I_ε are material constant related to the generalized inertial effects in the magnetic and mechanical fields, respectively.

Hence, the Lagrange function L can be constructed by using the potential and kinetic energy as:

$$L=U-V \tag{5}$$

Moreover, the dissipative effect in the process of martensite reorientation is also taken into consideration, and the generalized Rayleigh dissipation function is introduced as follows:

$$R=\frac{1}{2}\left(\tau_M\left(\frac{\mathrm{d}M}{\mathrm{d}t}\right)^2+\tau_\varepsilon\left(\frac{\mathrm{d}\varepsilon}{\mathrm{d}t}\right)^2\right), \tag{6}$$

where τ_M and τ_ε are material constant related to the generalized friction in the magnetic and mechanical field, respectively. It is easy to see this function is proportional to the square of the system states' change rate.

According to the Euler–Lagrange equation, the governing equations of the dynamic hysteresis can be obtained by using the following equations:

$$\frac{\mathrm{d}}{\mathrm{d}t}\frac{\partial L}{\partial \dot{M}}-\frac{\partial L}{\partial M}=\frac{\partial R}{\partial \dot{M}},\quad \frac{\mathrm{d}}{\mathrm{d}t}\frac{\partial L}{\partial \dot{\varepsilon}}-\frac{\partial L}{\partial \varepsilon}=\frac{\partial R}{\partial \dot{\varepsilon}}. \tag{7a-b}$$

Combining with the former Lagrange function, the temporal evolution equations of the system can be obtained as:

$$I_M\frac{\mathrm{d}^2M}{\mathrm{d}t^2}+\tau_M\frac{\mathrm{d}M}{\mathrm{d}t}+\frac{\partial\psi}{\partial M}=H,\quad I_\varepsilon\frac{\mathrm{d}^2\varepsilon}{\mathrm{d}t^2}+\tau_\varepsilon\frac{\mathrm{d}\varepsilon}{\mathrm{d}t}+\frac{\partial\psi}{\partial\varepsilon}=\sigma. \tag{8a-b}$$

These two equations contain the dynamic evolution process of the M and ε, which include the relaxation and inertial effects. Authors found that the influence of inertial effects on hysteresis is so small that it can be safely ignored for numerical approximation. Therefore, Eq. (8) can be simplified as the first-order form:

$$\tau_M\frac{\mathrm{d}M}{\mathrm{d}t}=-\frac{\partial\psi}{\partial M}+H,\tau_\varepsilon\frac{\mathrm{d}\varepsilon}{\mathrm{d}t}=-\frac{\partial\psi}{\partial\varepsilon}+\sigma. \tag{9a-b}$$

It is easy to see from Eq. (9) that the total energy of the system evolves to the minimum gradually, which is essentially consistent with the time-dependent Ginzburg–Landau theory [24, 26]. Substituting the expression of ψ, the governing equations of the system can be recast as:

$$\begin{aligned}&\tau_M\frac{\mathrm{d}M}{\mathrm{d}t}+A_2M+A_4M^3+A_6M^5+\beta\varepsilon M-H=0,\\&\tau_\varepsilon\frac{\mathrm{d}\varepsilon}{\mathrm{d}t}+k\varepsilon+\frac{bM^2}{2}-\sigma=0,\end{aligned} \tag{10a-b}$$

where τ_M and τ_ε represent the time constants of relaxation effect in the hysteresis process. The model presented above is expressed as two coupled nonlinear ordinary differential equations. The mechanical and magnetic fields are coupled intrinsically in the above model. Since the governing model is based on differential equations, it has great potential in many aspects, such as engineering control and energy harvesting [6, 13].

2.3 Model validation and discussions

To demonstrate that the proposed model can describe the hysteretic dynamics in the martensite reorientation process, the experiment results of 307 K in Ref. [9]

is adopted to validate the model. The MSMA specimen is $Ni_{49.7}Mn_{29.1}Ga_{21.2}$ single crystal. Compress stress of 1 MPa and a slowly changing external magnetic field varying between -1.15 and 1.15 T are applied to the specimen, which are perpendicular to each other. A relative magnetization is adopted as the ratio of the measured and the saturation magnetization, thus the unit of the magnetization in the experiment is 1.

In the numerical experiment, the applied magnetic field is assumed to vary linearly with the frequency $f_0 = 0.01$ Hz, and the units of the parameters are ignored. To be consistent with the experiment, Eq. (10a) is recast as:

$$\tau_m \frac{\mathrm{d}M}{\mathrm{d}t} + a_2 M + a_4 M^3 + a_6 M^5 + b\varepsilon M - \mu_0 H = 0, \tag{11}$$

where $\tau_m = \mu_0 \tau_M$, $a_2 = \mu_0 A_2$, $a_4 = \mu_0 A_4$, $a_6 = \mu_0 A_6$ and $b = \mu_0 \beta$. The parameters of the model are identified according to the experiment results, and the least square approximation method is used. Thus, the parameter identification problem can be transformed into a nonlinear least square optimization problem, and the goal function is adopted as:

$$\min G(\tau_m, \tau_\varepsilon, a_2, a_4, a_6, b, k) = \sum_{k=1}^{N} \left[\left(M_k - \tilde{M}_k\right)^2 + \left(\varepsilon_k - \tilde{\varepsilon}_k\right)^2 \right]. \tag{12}$$

In this equation, M_k are ε_k are the predicted values at kth time instant, respectively, while $\tilde{M}_k$ and $\tilde{\varepsilon}_k$ are the experimental counterparts. And $\tau_M, \tau_\varepsilon, a_2, a_4, a_6, b, k$ are the parameters needed to identify. In the above nonlinear optimization problems, the system is a nonlinear-evolution system, and the objective function G represents the global closeness, thus it is not applicable to use the gradient-based search methods. Considering this fact, the Nelder–Mead method [32] is used in this paper, which is a commonly used method for optimization problems lack gradient information of the goal function. The final optimized parameters are $\tau_m = 0.1, \tau_\varepsilon = 0.001, a_2 = 1.23, a_4 = -10.29, a_6 = 3.96, b = 1, k = -0.096$, and the model predictions and the experimental data are plotted in Fig. 4.

The RMS errors of the $\mu_0 H - M$ and $\mu_0 H - \varepsilon$ between the traditional Landau model and the experimental data are calculated as 0.11 and 0.49, respectively. It can be seen that the model can roughly capture the hysteretic dynamics trend of the experiment, but the result is not ideal. Therefore, we will revise the traditional model to improve its accuracy in the next section.

3 Improved model and validation

3.1 Improved differential model

As mentioned above, although the traditional Landau governing equations can simulate the hysteresis loops of MSMAs in principle, it is still not satisfactory and there is considerable room for improvement in the accuracy of the model. Therefore, in this section, the constitutive relation derived from Landau free energy function is improved, and the part $(a_2 M + a_4 M^3 + a_6 M^5)$ derived from the traditional Landau free energy is replaced by a new function $\phi_L(M)$, which will be determined next. Thus, the differential Eq. (11) is improved as:

$$\tau_M \frac{\mathrm{d}M}{\mathrm{d}t} + \phi_L(M) + b\varepsilon M - \mu_0 H = 0, \tag{13}$$

Referring to Sect. 2, it is found that τ_ε is much smaller than τ_m, which means the relaxation effect of the mechanical field in the hysteresis process is much smaller than that of

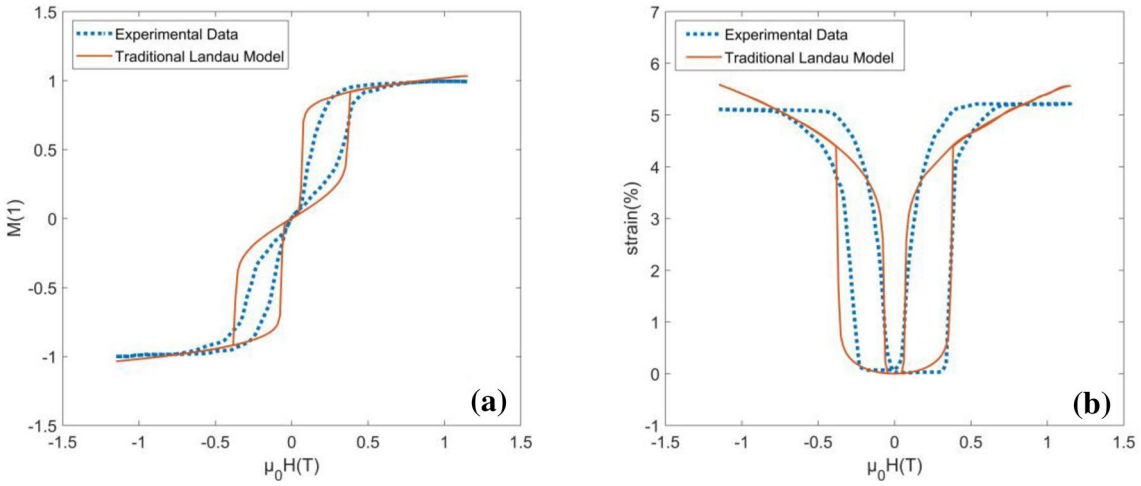

Fig. 4 Comparison of the model predictions using the traditional Landau model with the experimental data [9]. **a** $\mu_0 H - M$; **b** $\mu_0 H - \varepsilon$

the magnetic field. Thus, τ_ε is set to 0 for numerical approximation. Consequently, Eq. (10b) can be written as:

$$k\varepsilon + \frac{bM^2}{2} - \sigma = 0. \tag{14}$$

Combining Eqs. (13) and (14), it can be obtained as:

$$\tau_M \frac{\mathrm{d}M}{\mathrm{d}t} + F(M) - \mu_0 H = 0, \tag{15}$$

where

$$F(M) = \phi_L(M) - \frac{b^2}{2k}M^3 + \frac{b\sigma}{k}M. \tag{16}$$

Equation (15) is a first-order differential equation describing the $\mu_0 H - M$ relation, where $F(M)$ contains the effect of stress. In this section, $F(M)$ is adopted as a piecewise spline function constructed by parameters correlated with physical attributes of experiment results, and the threshold values are introduced according to Ref. [11] as shown in Fig. 5. $\mu_0 H^{s(1,2)}$, $\mu_0 H^{f(1,2)}$ and $\mu_0 H^{s(2,1)}$ correspond to the threshold values of the magnetic field in the forward ($V_1 \rightarrow V_2^+$) and reverse process ($V_2^+ \rightarrow V_1$), respectively, while $M^{s(1,2)}$ and $M^{s(2,1)}$ are the corresponding magnetization values. The symbols s and f, respectively, correspond to start and finish. Moreover, $\mu_0 H^{\max}$ denotes the maximum value of applied magnetic field, and M^{sat} is the saturation magnetization. The above values can be easily obtained from the hysteresis loop.

It can be seen from Fig. 5 that the curve of the $\mu_0 H - M$ is nearly symmetrical about the origin. According to Ref. [10], the hysteresis curves usually show asymmetry in the first cycle, but they will keep symmetry after the second cycle. It is worth noting that the experimental data point selected in this paper is the first cycle, so it will show a slight asymmetry. The proposed model is mainly used to describe the stable working state (after the second cycle) of materials. Thus, in the current paper, $F(M)$ is assumed as an odd function to make the $\mu_0 H - M$ curve symmetrical about the origin. If it is not an odd function, the curve presented will not be symmetric about the origin, which will increase the complexity and error of the model. Therefore, only the parameters larger than 0 are needed to be determined. With the help of the threshold values, the constitutive relation of the $F(M)$ can be obtained by using the cubic Hermite interpolation method. It is easy to see that $F(M)$ is non-convex, and bifurcations will be induced in the nonlinear dynamics leading to the hysteretic behavior [33]. After obtaining the expression of $F(M)$, $\phi_L(M)$ can be easily determined using Eq. (16) where the values of b, k are the same as that in Sect. 2.3, and σ is adopted as MPa. Above all, the improved differential model is composed of Eqs. (13) and (10b).

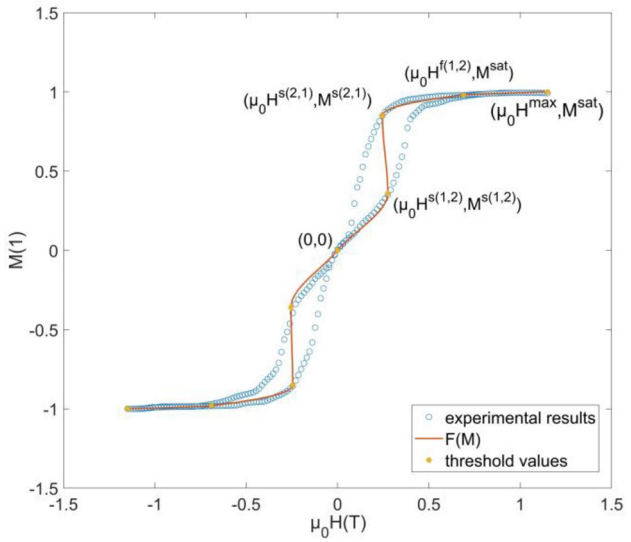

Fig. 5 Determination of the constitutive relation of $F(M)$

3.2 Model validation and discussions

To illustrate the superiority of the improved model, the hysteretic dynamic loops under 1 MPa is simulated as shown in Fig. 6a, b, in which the parameter values are taken from Ref. [9] as shown in Fig. 5. The experimental data are the same as in the previous section, and the Jiong et al. model in Ref. [34] is used for comparison.

It is clear that the effect of using the improved model is much better than that of the traditional model, especially in the $\mu_0 H - M$ curve. And the RMS errors of the improved model and Jiong et al. model compared with the experimental data are calculated, respectively. In $\mu_0 H - M$ curve, the RMS errors of the improved model and the Jiong et al. model are calculated as 0.050 and 0.10, respectively. And the corresponding RMS errors in $\mu_0 H - \varepsilon$ are 0.44 and 1.18, respectively. Therefore, it can be seen that the improved model is more accurate in this case. Then, change the applied stress to 0.8 MPa, and the prediction results of the improved model and Jiong et al. model are shown in Fig. 6c, d. As mentioned at the end of Sect. 3.1, since the experimental data are obtained in the first cycle, some curves will show asymmetry, especially in the low stress condition (0.8 MPa). And there will be a residual strain, but since the second cycle, the curve will become symmetrical [10]. In $\mu_0 H - M$ curve, the corresponding RMS errors are calculated as 0.058 and 0.092, respectively. And the corresponding RMS errors are, respectively, calculated as 0.98 and 0.79 in $\mu_0 H - \varepsilon$ curve. Therefore, it can be seen that this model can achieve high accuracy in magnetization prediction, but there are still shortcomings in strain prediction. All in all, it is undeniable that the improved model is generally satisfactory with a simple form and low calculation cost, which is very important in the engineering application.

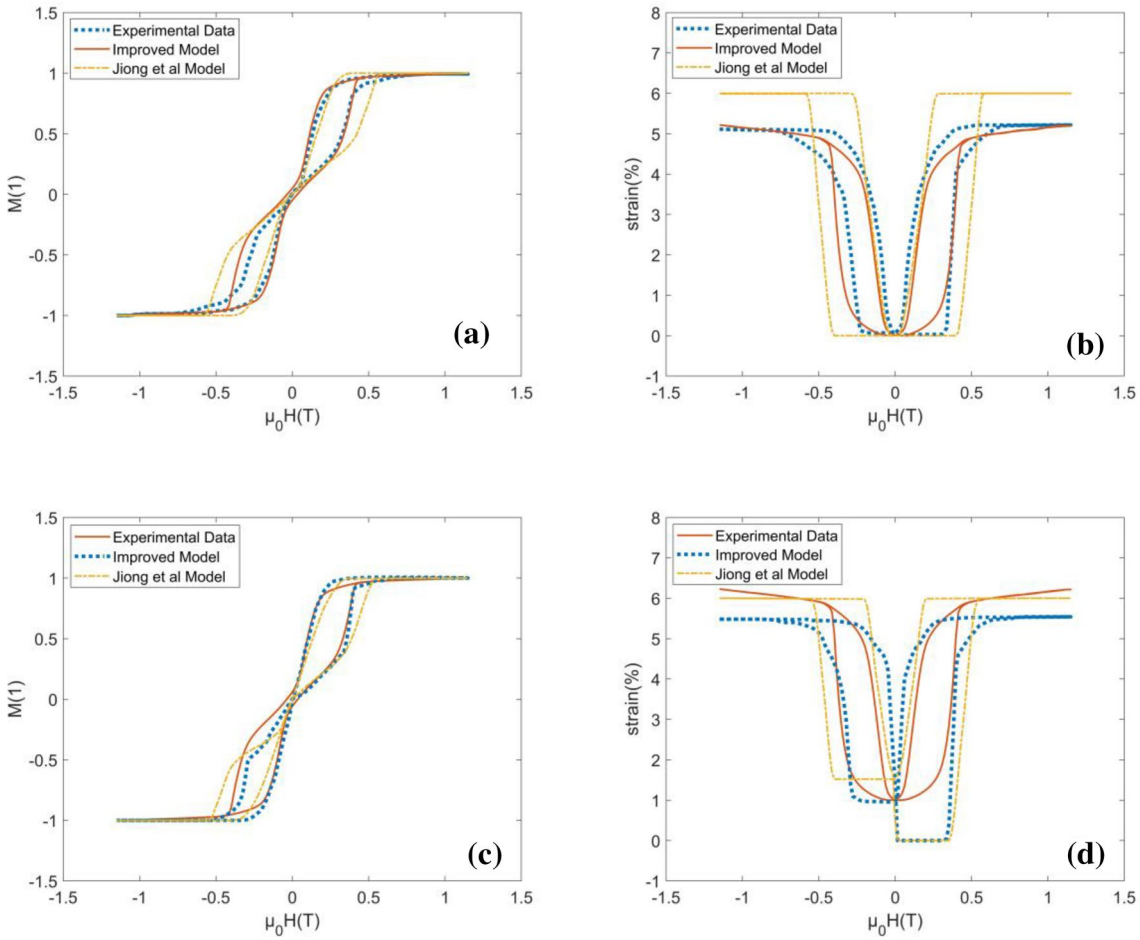

Fig. 6 Comparison of the model predictions using the improved model with Jiong et al. model [34] and experimental data [9]. **a** $\mu_0 H - M$ in 1 MPa; **b** $\mu_0 H - \varepsilon$ in 1 MPa; **c** $\mu_0 H - M$ in 0.8 MPa; **d** $\mu_0 H - \varepsilon$ in 0.8 MPa

Some inaccuracies in the model predictions can be rectified by other compensation algorithms afterward, which will be researched in our future works.

4 Frequency dependence

Compared with the static model, the frequency dependence of this dynamic model is inherently incorporated due to its differential nature, and the load ($\mu_0 H$) is included in the formula of the model. Thus, the output of the system will be affected by the load change rate. Taking the improved model as an example, the bias stress is 1 MPa, and other parameters are the same as those in Sect. 3.2, changing the frequency to $f_0/2$ and $2f_0$ ($f_0 = 0.01$ Hz), respectively. And the model predictions of the hysteresis curves are obtained as shown in Fig. 7.

It can be seen that with the increasing frequency, the curves become fatter and fatter, which is consistent with the trend of experiment results in Refs. [35, 36]. And when the frequency is $2f_0$ and H is 0, the value of ε is not zero. The main reason is that the frequency of the magnetic field is too high, and martensite variants do not have enough time to reorient. Thus there is a part of residual strain, which is similar to that of ferroelectric materials [17, 37, 38]. Therefore, it is necessary to have a part of the magnetic field to make the strain decrease to zero first, which is similar to the coercive field in ferroelectric materials. When the $\mu_0 H$ exceeds the coercive field, the strain value will jump as it continues to increase. Therefore, the curve will become fatter and fatter with the increasing frequency, and the proposed model can demonstrate the frequency dependence of MSMA commendably.

In order to further prove the frequency dependence of the model, we selected the model and the experimental data in Ref. [36] for comparison. The magnetic field ($\mu_0 H$) varies between − 1.2 and 1.2 T in the sinusoidal form. When the frequency of the magnetic field is 1 Hz, the model prediction of the improved model and Ronald et al. model in Ref. [36] are shown in Fig. 8a. And the RMS errors of the improved

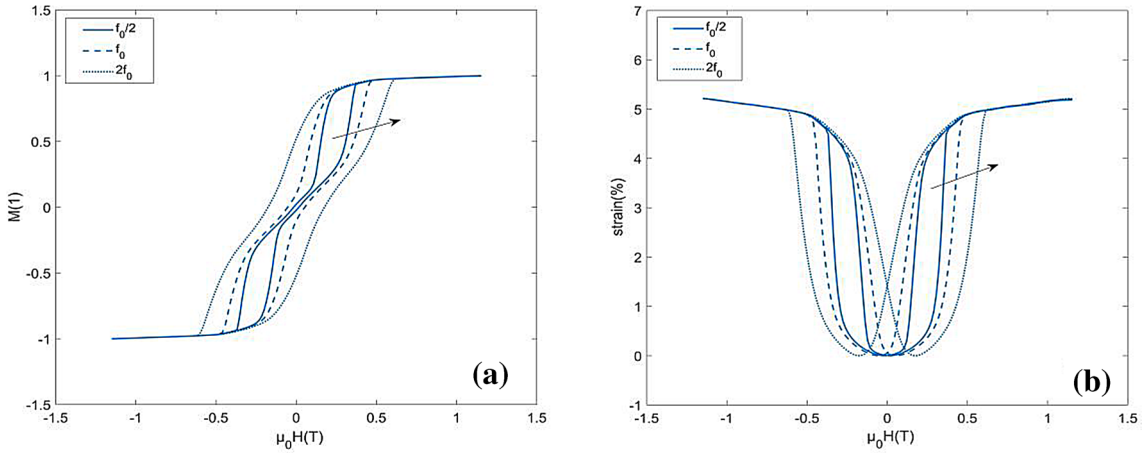

Fig. 7 Simulation of the system dynamics response under different frequencies where $f_0 = 0.01$ Hz. **a** $\mu_0 H - M$; **b** $\mu_0 H - \varepsilon$

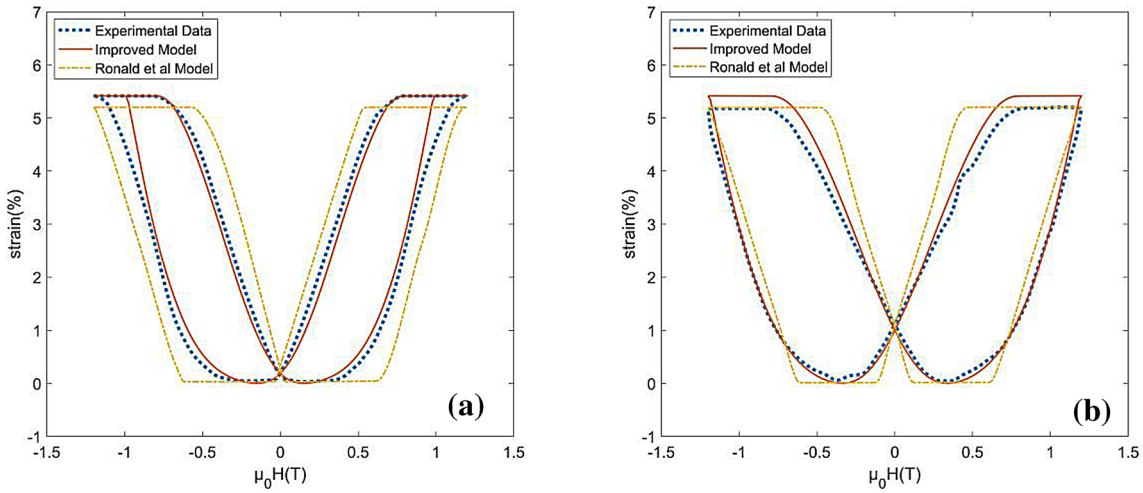

Fig. 8 Comparison of the model predictions using the improved model with Ronald et al. model [36] and experimental data [36]. **a** $\mu_0 H - \varepsilon$ in 1 Hz; **b** $\mu_0 H - \varepsilon$ in 2 Hz

model and the Ronald et al. model compared with the experimental data are calculated as 0.24 and 0.61, respectively. Then, change the frequency of the magnetic field to 2 Hz to get the predictions of the two models, as shown in Fig. 8b. Besides, the RMS errors of the improved model and the Ronald et al. model are calculated as 0.21 and 0.54, respectively. Therefore, the frequency dependence of the model is further validated.

5 Feedback linearization and validation

5.1 Feedback methodology

Because the theories for the system described by linear ordinary differential equations in dynamics analysis and controller design are well developed, using a specific linear system to approximate or associate the hysteresis dynamics is an important way to deal with the control difficulties in our system in engineering applications [39]. Since the bifurcation problems caused by the nonlinearity in dynamic systems are needed to deal with, the traditional method of using Taylor expansion to approximate the nonlinear systems is not feasible here [40].

In this section, an approach based on the nonlinear feedback method is used to compensate for the initial system hysteresis, and consequently, the system is linearized effectively. The essence of this feedback linearization is that nonlinear feedback consisted of the system states is introduced to compensate the initial nonlinear part.

Take the improved model as an example, first, the differential model is recast into the following state space:

$$\boldsymbol{\tau}\dot{\boldsymbol{x}} = \boldsymbol{l}(\boldsymbol{x}) + \boldsymbol{n}(\boldsymbol{x}) + \boldsymbol{u},$$
$$\boldsymbol{x} = \begin{bmatrix} M \\ \varepsilon \end{bmatrix}, \boldsymbol{\tau} = \begin{bmatrix} \tau_m & 0 \\ 0 & \tau_\varepsilon \end{bmatrix}, \boldsymbol{l}(\boldsymbol{x}) = \begin{bmatrix} 0 & 0 \\ 0 & -k \end{bmatrix}\boldsymbol{x}, \boldsymbol{n}(\boldsymbol{x}) = -\begin{bmatrix} \phi_L(M) + b\varepsilon M \\ bM^2/2 \end{bmatrix}, \boldsymbol{u} = \begin{bmatrix} \mu_0 H \\ \sigma \end{bmatrix}. \tag{18}$$

It is obvious that the state space consisted of two separated parts: linear ($\boldsymbol{l}(\boldsymbol{x})$) and nonlinear ($\boldsymbol{n}(\boldsymbol{x})$) part. The basic principle of feedback linearization is to transform the original system into a linear system by eliminating its nonlinear part [41]. For linearization, the new input of the feedback linearization system is chosen as $\boldsymbol{v} = \left[\mu_0 H_n(t), \sigma_n(t)\right]^T$. Therefore, the input of the initial stem is assumed to be composed as [41]:

$$\boldsymbol{u} = \boldsymbol{K}_N(\boldsymbol{M}, \boldsymbol{\varepsilon}) + \boldsymbol{\tau}\boldsymbol{v},$$
$$\boldsymbol{K}_N(\boldsymbol{M}, \boldsymbol{\varepsilon}) = \boldsymbol{\tau}_n\boldsymbol{x} - \boldsymbol{n}(\boldsymbol{x}) = \begin{bmatrix} -\tau_m & 0 \\ 0 & -\tau_\varepsilon + k \end{bmatrix}\begin{bmatrix} M \\ \varepsilon \end{bmatrix} + \begin{bmatrix} \phi_L(M) + b\varepsilon M \\ bM^2/2 \end{bmatrix}, \tag{19}$$

where $\boldsymbol{K}_N(\boldsymbol{M}, \boldsymbol{\varepsilon})$ is responsible for the nonlinear feedback as mentioned above. It is worth noting that $\boldsymbol{K}_N(\boldsymbol{M}, \boldsymbol{\varepsilon})$ contains the opposite sign of the nonlinear part of the original system. The corresponding control block diagram of system feedback linearization is shown in Fig. 9a. The dotted line represents the feedback part.

Obviously, the hysteresis dynamics in the initial system is naturally eliminated, and in this way, the system can be transformed into a linear system for the new input $\boldsymbol{v}$:

$$\boldsymbol{\tau}\dot{\boldsymbol{x}} = \boldsymbol{A}\boldsymbol{x} + \boldsymbol{B}\boldsymbol{v},$$
$$\boldsymbol{A} = \begin{bmatrix} -\tau_m & 0 \\ 0 & -\tau_\varepsilon \end{bmatrix}, \boldsymbol{B} = \begin{bmatrix} \tau_m & 0 \\ 0 & \tau_\varepsilon \end{bmatrix}, \tag{20}$$

which can be recast as two decoupled equations:

$$\frac{\mathrm{d}M}{\mathrm{d}t} = -M + \mu_0 H_n, \quad \frac{\mathrm{d}\varepsilon}{\mathrm{d}t} = -\varepsilon + \sigma_n. \tag{21a-b}$$

The corresponding control block diagram of the linearization system is shown in Fig. 9b. The correspondence between the transformed linear system and the initial system is clarified, and it is feasible to use the linear control system analysis and design. Therefore, the corresponding input $\boldsymbol{v}$ can be determined according to the desired state variables ($\boldsymbol{x}$) trajectory. Then the input of the initial hysteresis system can be obtained by Eqs. (19) and (21) directly. Hence, it can be seen that the hysteresis in the control system can be overcome by using the proposed method. Undoubtedly, the success of the proposed methodology is mainly due to the differential form of our model.

5.2 Validation and discussion

In this section, a numerical experiment is presented to demonstrate that the required input to drive the system in the desired trajectory can be easily calculated by using the proposed methodology. Here, we assume to drive M linearly from -1 to 1 and then back to -1 in one period ($f_0 = 0.01$ Hz) at 1 MPa stress. The parameters of the model are consistent with those in Sect. 3. For simplicity, we have no requirement for ε, thus the initial system model is chosen as Eq. (15). Thus, the task is to calculate the actual input $\mu_0 H(t)$ for the system (Eq. (15)).

First, as mentioned above, the input $\mu_0 H(t)$ can be divided into two parts:

$$\mu_0 H(t) = K_N(M) + K_L(M)\mu_0 H_n(t). \tag{22}$$

and $K_N(M)$ and $K_L(M)$ can be set as follows:

$$K_N(M) = -\tau_m M + F(M), K_L(M) = \tau_m, \tag{23}$$

which are simplified from Eq. (19). Take the input $\mu_0 H(t)$ into the system (Eq. (15)) and simplify it, the linear system is obtained as Eq. (21a) shows, consequently.

In the linear system Eq. (21a), since the expression of the desired M is defined, and it is derivable, the $\frac{\mathrm{d}M}{\mathrm{d}t}$ is easy to obtain. Thus, the expression of the new input $\mu_0 H_n(t)$ can be calculated easily as:

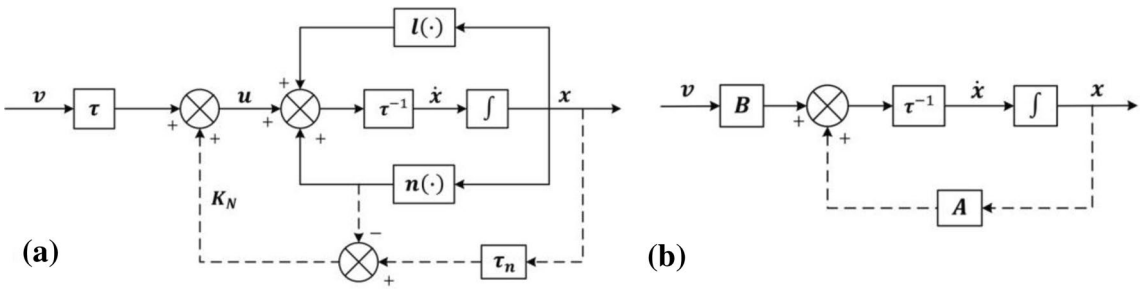

Fig. 9 Control block diagram of the system. **a** Feedback linearization methodology; **b** Corresponding linearization system

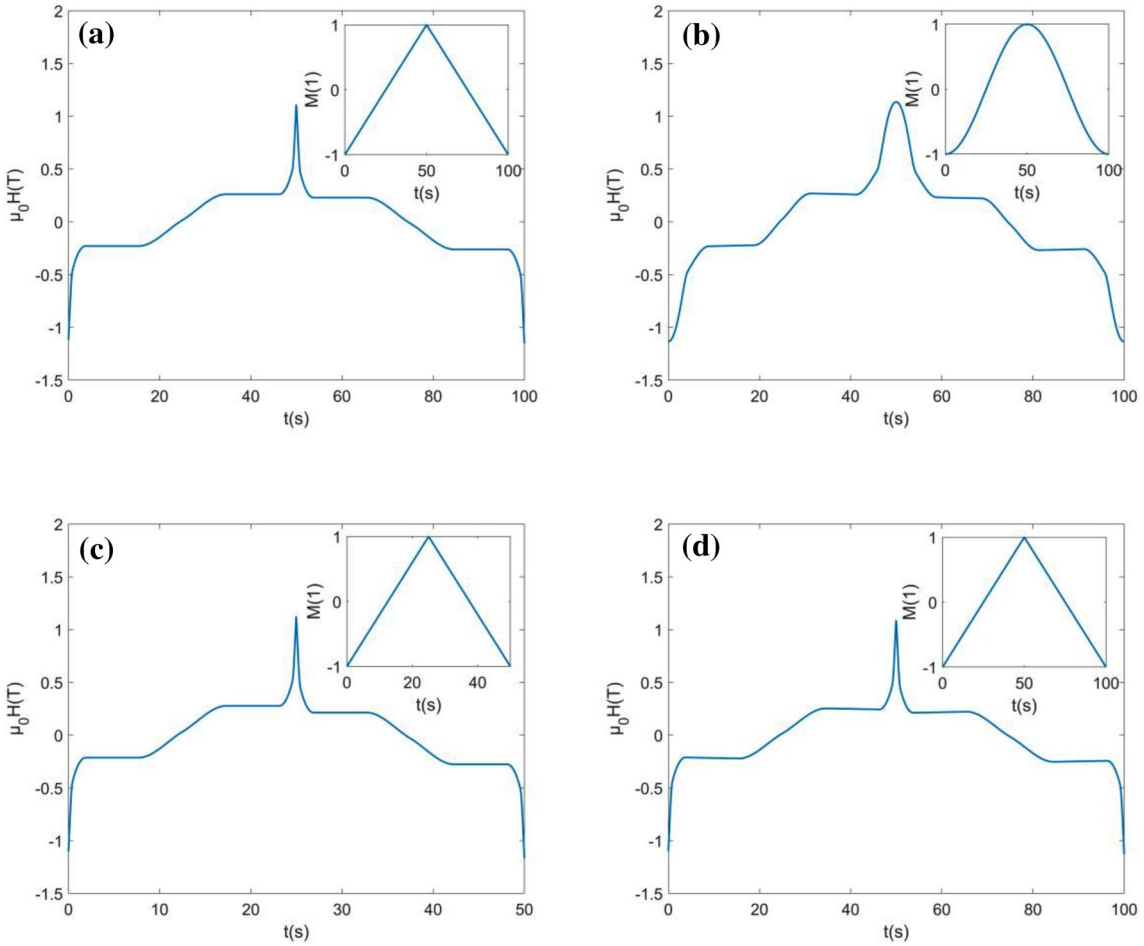

Fig. 10 Numerical results of the inputs and outputs for the system using feedback linearization methodology. **a** Linear output, $f_0 = 0.01$ Hz, $\sigma = 1$ MPa; **b** Sinusoidal output, $f_0 = 0.01$ Hz, $\sigma = 1$ MPa; **c** Linear output, $f_0 = 0.02$ Hz, $\sigma = 1$ MPa; **d** Linear output, $f_0 = 0.01$ Hz, $\sigma = 0.8$ MPa.

$$\mu_0 H_n(t) = \frac{\mathrm{d}M}{\mathrm{d}t} + M. \tag{24}$$

Then the real input $\mu_0 H(t)$ can be obtained using the Eqs. (22) and (23) with the calculated $\mu_0 H_n(t)$ consequently and is shown in Fig. 10a. Moreover, take $\mu_0 H_n(t)$ into the original system and the output M is obtained as shown in the top right corner of Fig. 10a. It can be seen from the figure that M satisfies the desires trajectory well, which proves the feasibility of this method. Then, we assume that the desired output M is sinusoidal with the same frequency as before. The corresponding input is calculated, and it is brought into the system to get the corresponding output, as shown in Fig. 10b. After that, keeping other conditions consistent with Fig. 10a, we change the input frequency to 0.02 Hz and the applied stress to 0.8 MPa, respectively. Then. the corresponding inputs are calculated and brought into the system to calculate the actual output. The results are shown in Fig. 10c, d. It can be seen from Fig. 10 that the feedback linearization methodology can meet the needs well and get the desired output. In addition, if the desired trajectory of M has other forms and requirements, the input $\mu_0 H(t)$ can be calculated using the same method.

From the above numerical experiments, it can be seen that the proposed methodology is effective. The traditional method of controlling hysteresis is to find the inverse of the model, which is very complicated [42]. In order to control the hysteretic dynamics, we divide the input of the system into two parts: one is the nonlinear feedback part to cancel the original hysteretic dynamics, and the other is the input of the corresponding linear system calculated according to the requirements. In other words, the hysteretic part of the original dynamics is compensated by the hysteretic behavior introduced by the nonlinear feedback as a part of the input, which greatly simplifies the design of the hysteretic control system.

6 Conclusion

In the current paper, a differential model is proposed based on the Landau theory of phase transition to describe the hysteresis in MSMAs. First, the three-dimensional structure is simplified into a one-dimensional model with three martensitic orientations. A non-convex Landau free energy function with three local minima corresponding to three martensite orientations is constructed. On this basis, the Lagrange and Rayleigh dissipation function of the system are introduced. Then, according to the Euler-Lagrange equation, the traditional model is obtained and compared with the experimental data. However, the accuracy of this model is not ideal. Thus, an improved model is proposed to improve the accuracy, in which the parameters are easily measured in the experiment curve. Numerical experiments show that the accuracy of the improved model is higher than that of the traditional Landau model and one proposed model in reference. Then, changing the applied stress value, it is found that the model can still predict the corresponding hysteretic behavior well. Moreover, the improved model shows its superiority in frequency dependence due to its differential form. It successfully describes the hysteresis characteristics of MSMA at different frequencies and has higher accuracy than the chosen existing model. Finally, a feedback linearization methodology is proposed by introducing a compensation term to eliminating its nonlinear part. Thus, the original system is transformed into a linear system, and the outputs of the system can develop in the desired trajectory. Moreover, we change the applied stress, frequency, and the form of the desired output, respectively. Then the corresponding inputs are calculated and brought into the system. It is found that the actual output can satisfy the requirements, which further shows the superiority of that differential model.

Acknowledgments This work was supported by the National Natural Science Foundation of China (Grant Nos. 51575478 and 61571007).

References

1. K. Ullakko et al., Large magnetic-field-induced strains in Ni2MnGa single crystals. Appl. Phys. Lett. **69**(13), 1966–1968 (1996)
2. D.C. Lagoudas, *Shape Memory Alloys: Modelling and Engineering Applications* (Springer-Verlag, New York, NY, 2008).
3. S.J. Murray et al., 6% Magnetic-field-induced strain by twin-boundary motion in ferromagnetic Ni–Mn–Ga. Appl. Phys. Lett. **77**(6), 886–888 (2000)
4. L. Hirsinger, N. Creton, C. Lexcellent, Stress-induced phase transformations in Ni–Mn–Ga alloys: experiments and modelling. Mater. Sci. Eng. A Struct. Mater.: Prop. Microstruct. Process. **378**(1), 365–369 (2004)
5. P. Müllner, V.A. Chernenko, G. Kostorz, Large cyclic magnetic-field-induced deformation in orthorhombic (14M) Ni–Mn–Ga martensite. J. Appl. Phys. **95**(3), 1531–1536 (2004)
6. I. Karaman et al., Energy harvesting using martensite variant reorientation mechanism in a NiMnGa magnetic shape memory alloy. Appl. Phys. Lett. **90**(17), 172505 (2007)
7. H.E. Karaca et al., Stress-induced martensite to austenite phase transformation in Ni2MnGa magnetic shape memory alloys. Smart Mater. Struct. **21**(4), 45011 (2012)
8. M.A.A. Farsangi et al., Energy harvesting from structural vibrations of magnetic shape memory alloys. Appl. Phys. Lett. **110**(10), 103905 (2017)
9. L. Straka, O. Heczko, S. Hannula, Temperature dependence of reversible field-induced strain in Ni–Mn–Ga single crystal. Scr. Mater. **54**(8), 1497–1500 (2006)
10. B. Kiefer et al., Characterization and modeling of the magnetic field-induced strain and work output in Ni2MnGa magnetic shape memory alloys. J. Magn. Magn. Mater. **312**(1), 164–175 (2007)
11. B. Kiefer, D.C. Lagoudas, Magnetic field-induced martensitic variant reorientation in magnetic shape memory alloys. Philos. Mag. **85**(33–35), 4289–4329 (2005)
12. H. Shi et al., Numerical modeling of magnetomechanical characteristics of Ni–Mn–Ga magnetic shape memory alloy. IEEE Trans. Magn. **55**(11), 1–9 (2019)
13. N.M. Bruno et al., A theoretical and experimental investigation of power harvesting using the NiMnGa martensite reorientation mechanism. Smart Mater. Struct. **21**(9), 94018 (2012)
14. H.E. Karaca et al., Magnetic field and stress induced martensite reorientation in NiMnGa ferromagnetic shape memory alloy single crystals. Acta Mater. **54**(1), 233–245 (2006)
15. M.A.A. Farsangi, H. Zohoor, Acoustic energy harvesting via magnetic shape memory alloys. J. Phys. D Appl. Phys. **52**(13), 135501 (2019)
16. L. Wang, R. Melnik, F. Lv, Stress induced polarization switching and coupled hysteretic dynamics in ferroelectric materials. Front. Mech. Eng. **6**(3), 287–291 (2011)
17. H. Du et al., Investigation on energy dissipation by polarization switching in ferroelectric materials and the feasibility of its application in sound wave absorption. Appl. Phys. A Mater. Sci. Process. **126**(2), 1–15 (2020)
18. A. Agneni, F. Mastroddi, G.M. Polli, Shunted piezoelectric patches in elastic and aeroelastic vibrations. Comput. Struct. **81**(2), 91–105 (2003)
19. J. Wang, P. Steinmann, A variational approach towards the modeling of magnetic field-induced strains in magnetic shape memory alloys. J. Mech. Phys. Solids **60**(6), 1179–1200 (2012)
20. H. Sayyaadi, M.A.A. Farsangi, Frequency-dependent energy harvesting via magnetic shape memory alloys. Smart Mater. Struct. **24**(11), 115022 (2015)
21. R. Xu, M. Zhou, Elman neural network-based identification of Krasnosel'Skii-Pokrovskii model for magnetic shape memory alloys actuator. IEEE Trans. Magn. **53**(11), 1–4 (2017)
22. Y. Yu, C. Zhang, M. Zhou, NARMAX model-based hysteresis modeling of magnetic shape memory alloy actuators. IEEE Trans. Nanotechnol. **19**, 1–4 (2020)
23. F. Falk, Landau theory and martensitic phase transitions. Le Journal de Physique Colloques **43**(C4), C4–C3 (1982)
24. D. Wang, L. Wang, R. Melnik, A differential algebraic approach for the modeling of polycrystalline ferromagnetic hysteresis with minor loops and frequency dependence. J. Magn. Magn. Mater. **410**, 144–149 (2016)
25. L.X. Wang et al., Extension of the Landau theory for hysteretic electric dynamics in ferroelectric ceramics. J. Electroceram. **24**(1), 51–57 (2010)

26. M.S. Richman, P. Rulis, A.N. Caruso, Ferroelectric system dynamics simulated by a second-order Landau model. J. Appl. Phys. **122**(9), 94101 (2017)
27. H.S. Park et al., Behavior of magnetic domains during structural transformations in Ni2MnGa ferromagnetic shape memory alloy. Appl. Phys. Lett. **83**(18), 3752–3754 (2003)
28. A. Berti, C. Giorgi, E. Vuk, Hysteresis and temperature-induced transitions in ferromagnetic materials. Appl. Math. Model. **39**(2), 820–837 (2015)
29. A.N. Vasil'ev et al., Shape memory ferromagnets. Phys. Uspekhi **46**(6), 559–588 (2003)
30. X. He et al., Modelling ageing phenomenon in ferroelectrics via a Landau-type phenomenological model. Smart Mater. Struct. **30**(1), 015017 (2020)
31. F. Falk, Model free energy, mechanics, and thermodynamics of shape memory alloys. Acta Metall. **28**(12), 1773–1780 (1980)
32. L. Wang, M. Willatzen, Modeling of nonlinear responses for reciprocal transducers involving polarization switching. IEEE Trans. Ultrason. Ferroelectr. Freq. Control **54**(1), 177–189 (2007)
33. L.X. Wang, M. Willatzen, Nonlinear dynamical model for hysteresis based on nonconvex potential energy. J. Eng. Mech. **133**(5), 506–513 (2007)
34. J. Wang, P. Steinmann, Finite element simulation of the magneto-mechanical response of a magnetic shape memory alloy sample. Philos. Mag. **93**(20), 2630–2653 (2013)
35. N. Sarawate, M. Dapino, Frequency dependent strain-field hysteresis model for ferromagnetic shape memory Ni-Mn-Ga. IEEE Trans. Magn. **44**(5), 566–575 (2008)
36. R.N. Couch J. Sirohi, I. Chopra. Testing and Modeling of NiMnGa Ferromagnetic Shape Memory Alloy for Static and Dynamic Loading Conditions, vol. 6173. SPIE (2006). https://doi.org/10.1117/12.659665.
37. W. Eerenstein, N.D. Mathur, J.F. Scott, Multiferroic and magnetoelectric materials. Nature (London) **442**(7104), 759–765 (2006)
38. X. He et al., Modelling of creep hysteresis in ferroelectrics. Philos. Mag. (Abingdon, England) **98**(14), 1256–1271 (2018)
39. L. Wang, R.V.N. Melnik, Control of coupled hysteretic dynamics of ferroelectric materials with a Landau-type differential model and feedback linearization. Smart Mater. Struct. **18**(7), 074011 (2009)
40. W.M. Haddad, V. Chellaboina, *Nonlinear Dynamical Systems and Control: A Lyapunov-Based Approach* (Princeton University Press, Princeton, 2011).
41. J.-J.E. Slotine, W. Li, *Applied Nonlinear Control, No. 1*, vol. 199 (Prentice hall, Englewood Cliffs, NJ, 1991).
42. V. Hassani, T. Tjahjowidodo, T.N. Do, A survey on hysteresis modeling, identification and control. Mech. Syst. Signal Process. **49**(1–2), 209–233 (2014)